Polymer Degradation and Stability 159 (2019) 153–162

Contents lists available at ScienceDirect

Polymer Degradation and Stability

journal homepage: www.elsevier.com/locate/polydegstab

Facile fabrication of biobased P–N–C-containing nano-layered hybrid: Preparation, growth mechanism and its efficient fire retardancy in epoxy

Peng-Ji Wang [a, 1], Dui-Jun Liao [a, 1], Xiao-Ping Hu [a, d, *], Ning Pan [b], Wen-Xiong Li [a], De-Yi Wang [c, **], Yong Yao [d]

[a] State Key Laboratory for Environment-friendly Energy Materials, School of Materials Science and Engineering, Southwest University of Science and Technology, Mianyang, 621010, PR China
[b] Fundamental Science on Nuclear Wastes and Environmental Safety Laboratory, Southwest University of Science and Technology, Mianyang, 621010, PR China
[c] IMDEA Materials Institute, C/Eric Kandel, 2, 28906, Getafe, Madrid, Spain
[d] Shock and Vibration of Engineering Materials and Structures Key Laboratory of Sichuan Province, Mianyang, 621000, PR China

ARTICLE INFO

Article history:
Received 5 September 2018
Received in revised form
21 November 2018
Accepted 25 November 2018
Available online 27 November 2018

Keywords:
Phytic acid
Nano-layered
Self-assembly
Multi-functional
Fire-retardant
Epoxy resin

ABSTRACT

A bio-based organic-inorganic hyperbranched hybrid (PAMA), possessing unique nano-layered structure, was designed and prepared by the neutralization reaction between phytic acid and melamine, then used as a multi-function intumescent flame retardant for epoxy resin (EP). FTIR, ^{1}H NMR, XRD, XPS, TGA and DSC were employed to investigate the chemical structure, growth mechanism and thermal behaviour of PAMA. SEM and TEM results confirmed the nano-layered structure of the PAMA. The limiting oxygen index (LOI) of EP incorporated with 6 wt% PAMA (EP-6) was 29.7%, and the UL-94 V-0 rating was also achieved. In contrast to the EP, the peak heat release rate (PHRR), total smoke production (TSP), and fire growth rate (FIGRA) of EP-6 were reduced by 62.3, 36.2, and 62.16%, respectively. The flame retardant mechanism of PAMA was further depicted using TG-FTIR and SEM/EDX techniques. In addition, the mechanical properties of EP composites are reinforced by the incorporation of PAMA. All the results demonstrate that the nano-layered PAMA is a high-efficient and eco-friendly fire retardant for EP.

1. Introduction

Epoxy resin (EP) is one of the most important thermosetting polymers, which is widely used in electrical and electronic materials, transportation and aerospace industry, laminates and composite applications, due to its easy moulding, high thermal, mechanical stabilities, chemical resistance and strong adherence [1–5]. However, the high flammability of epoxy resin greatly confines its application areas where needed high fire requirement. Many strategies have been developed to improve the fire retardancy of epoxy resin, including halogen-containing fire retardants, Intumescent fire retardants (IFRs), carbon nanomaterials and LDH, etc. [6–11].

In which, IFRs have been long-term developed and attracted numerous attentions due to the unparalleled environmentally friendliness and high-efficiency [12,13]. In general, a typical intumescent system should involve in three components: acid source, carbon source, and gas source [14]. In most cases, the intumescent fire retardants contain ammonium polyphosphate (APP), melamine (MA) and melamine polyphosphate (MPP). However, the poor compatibility between IFR and polymer matrix exists inevitably, which should seriously deteriorate the mechanical properties and lower the flame-retardant efficiency in EP. To address these problems, a good approach is combining the three components into one molecule, especially producing the polymeric IFR [15]. What is more, it is a preferential pathway by introducing organic groups into the polymeric IFR molecule, which will largely improve the

* Corresponding author. State Key Laboratory for Environment-friendly Energy Materials, School of Materials Science and Engineering, Southwest University of Science and Technology, Mianyang, 621010, PR China.
** Corresponding author. IMDEA Materials Institute, C/Eric Kandel, 2, 28906 Getafe, Madrid, Spain.
E-mail addresses: huxiaoping@swust.edu.cn (X.-P. Hu), deyi.wang@imdea.org (D.-Y. Wang).
[1] These authors contributed equally to this work.

https://doi.org/10.1016/j.polymdegradstab.2018.11.024
0141-3910/

compatibility of IFR in the polymer matrix.

Nowadays, the environmental footprint of IFRs is a key factor that must be concerned. Some biodegradable components in IFRs have been particularly designed and prepared such as mainly lignins, seaweed and starch [16–18]. Phytic acid (PA), mainly originating from cereal grains, beans and oilseeds, is a natural, eco-friendly, biodegradable and phosphorus-rich acid [19,20]. From the point of a flame-retardant perspective, the phytic acid molecule can provide an effective acid source and a carbon source, simultaneously. In addition, phytic acid is an organic acid, which would be beneficial to the dispersion property of the phytic acid derivatives in the polymer matrix.

Melamine and its salt were widely used as a fire retardant, especially in the intumescent system [15,21,22]. It is known that melamine can produce lots of non-flammable nitrogen-containing compounds such as NH_3, N_2 and NO_2 during the combustion, which could dilute the combustible volatiles [23,24]. The research has also shown that melamine undergoes progressive condensation on heating with the elimination of ammonia, and then forming the more thermally stable polymeric products such as melam and melem, which could contribute to the formation of more char residue [25]. Thus, integrating the advantages of phytic acid and MA into one molecule may be a promising candidate for traditional intumescent flame retardants. However, the flame retardant efficiency is usually affected by the aggregation structure and size of the flame retardant. In general, the well-dispersion of flame retardant with nano-structure shows excellent properties, including improved mechanical. For example, non-organic nano-layered materials, such as montmorillonite (MMT) [26,27], layered double hydroxides (LDHs) [28–31] and graphene nanosheets (GNSs) [32–35], have attracted much attention in recent years due to its "barrier" effect during combustion and its reinforcing function. However, an organic modification for nano-layered materials is absolutely necessary to obtain better compatibility in the polymer matrix. It is desirable to incorporating organic unit into nano-layered flame retardant in one-step synthesis process, avoiding complicated modification procedure and reducing the cost of material preparation.

Based on the inspiration of above-mentioned research, a unique bio-based organic-inorganic hybrid (PAMA) was first time designed and prepared combining phytic acid with melamine, which is of hyperbranched nano-layered structure, and possesses an acid source, a carbon source and a gas source, simultaneously. The chemical structure and morphology of PAMA were characterized by FTIR, ^{1}H NMR, XPS, EDX mapping, SEM and TEM, and a possible growth mechanism of the nano-layered structure is presented. The thermal stability, fire retardancy and the flame retardant mechanism of PAMA in EP were comprehensively investigated using different measurements.

2. Experimental

2.1. Materials

Phytic acid (PA, 70 wt% solution in H_2O), ethanol and metaphenylene diamine were obtained from Aladdin Chemistry Co., Ltd. Melamine was purchased from Chengdu Kelong Chemical Reagent Factory and used without further purification. Epoxy resin (Di-Glycidyl Ether of Bisphenol A, DGEBA, E−44, with an epoxy value of 0.41–0.48) was provided by Nantong Star Material Synthetic Co., Ltd.

2.2. Preparation of nano-layered PAMA

The nano-layered PAMA was synthesized employing the hydrothermal method by adjusting the molar ratio, pH value and reaction temperature. In brief, 3.7 mL (0.005 mol) phytic acid and 3.78 g (0.03 mol) melamine were added in the 100 mL of deionized water, and stirred at room temperature for 30 min to obtain the homogeneous mixture. Subsequently, the mixture was transferred into a 200 mL Teflon-lined autoclave. The autoclave was sealed and heated to 80 °C for 48 h. After cooling, the final product was filtered and washed several times with distilled water and ethanol until the pH value was around 7.0. The resultant white solid product (named as PAMA) was dried in vacuum oven at 60 °C to a constant weight. It is very important that the PAMA is almost water-insoluble under 55 °C.

2.3. EP composite samples preparation

A series of EP composites with different loadings of PAMA were prepared, and the corresponding formulations are listed in Table 1. The detailed preparation process can be described as following: EP and PAMA with various mass ratios were blending with acetone under ultrasonication of 150 W for 20 min, next, placed in a rotary evaporator at 80 °C to remove the acetone solvent. Afterwards, the appropriate amount of m-Phenylenediamine (m-PDA) was poured into the above mixture and stirred until m-PDA was totally dissolved, then degassed under a vacuum at 80 °C until no bubbles emerged. Subsequently, the viscous liquid was immediately poured into the preheated polytetrafluoroethylene mould, and the curing procedure was set as the procedure of 80 °C/3 h, 100 °C/2 h, and 120 °C/3 h. After cooling to room temperature gradually, the standard fire retardant samples for various tests were prepared.

2.4. Materials characterization

X-ray diffractometer (XRD) patterns were collected by D/max-1400 X-ray diffractometer equipped with a Cu-Kα radiation ($\lambda = 1.541$ Å) at a scanning rate of 2° per second in the 2θ range of 3–50°. Fourier transform infrared spectra (FTIR) were obtained on a Perkin Elmer Spectrum One spectrophotometer with a scanning range from 4000 to 400 cm^{-1} and using KBr discs. ^{1}H NMR (600 MHz) was performed on Bruker Avance 600 spectrometer, using DMSO-d_6 as a solvent. The surface morphologies and composition of the PAMA and MA were carried on a Ultra55 scanning electron microscope (SEM) accompanied energy-dispersive X-ray (EDX) analysis. The PAMA powder was ultrasonically dispersed in ethanol and then dropped onto a conducting copper tape. The morphology and microstructures of PAMA were observed on a Libra200 transmission electron microscopy (TEM) (Carl Zeiss irts, Germany) at an accelerated voltage of 200 kV. The fracture surface of EP/PAMA composites and the char formed after cone calorimetry were investigated using SEM. Elemental analysis of the chars was also investigated by energy-dispersive X-ray (EDX) analyzer at an accelerating voltage of 15 kV. All samples were sputter coated with a thin platinum layer before the examination.

Table 1
Detailed formulation and fire retardancy of various EP/PAMA composites.

Samples	EP/wt%	PAMA/wt%	Fire retardancy	
			LOI/%	UL-94 (3.2 mm)
EP-0	100	0	24.0 ± 0.3	NR
EP-4	96	4	25.6 ± 0.4	NR
EP-5	95	5	27.8 ± 0.3	V-1
EP-6	94	6	29.7 ± 0.1	V-0
EP-7	93	7	30.6 ± 0.2	V-0

X-ray photoelectron spectroscopy (XPS) of PAMA and MA were obtained by a XSAM80 (Kratos Co., U.K.), using Al Kαexcitation radiation (hν = 1486.6 eV). The flammability of the sample was investigated by using a cone calorimeter (Fire Testing Technology, UK) according to ISO 5660. The samples with 100 × 100 × 3 mm^3 were irradiated at a heat flux of 35 kW m^{-2}. The measurements were done in triplicate and the average data were reported. Limiting oxygen index (LOI) was measured with a JF-3 oxygen index meter according to ASTM D 2863-97 with test strips of dimensions 130 × 6.5 × 3.2 mm^3. UL-94 vertical burning test recorded an instrument (Nanjing Jionglei Instrument Equipment Co., Ltd.), according to ASTM D 3801 standard and the specimens for testing were of dimensions 130 × 13 × 3.2 mm^3. Thermogravimetric (TG) analysis was carried out by a STA6000 simultaneous thermal analyzer (PerkinElmer, USA) with a heating rate of 10 °C/min in nitrogen with the temperatures range from 40 to 700 °C. TG-FTIR spectra were recorded on STA6000 simultaneous thermal analyzer (PerkinElmer, USA) from 40 to 700 °C under a nitrogen atmosphere. The glass transition temperatures (T_g) of EP and its composite were investigated by differential scanning calorimetry (DSC) using a DSCQ2000 (TA Instrument company, USA). An ETM105D 100 KN computer-controlled electronic universal testing machine (WANCE GROUP) was utilized to measure the tensile strength on the dumbbell-shaped specimens at 20 mm/min test speed, complying with GB/T 1040.3–2006. The non-notched impact tests were performed on a PIT501J LCD plastic Charpy impact testing machine (Shenzhen million Test Equipment Co., Ltd.) with dimensions of 80.0 × 10.0 × 4.0 mm^3, according to GB/T 1043-2008.

3. Results and discussion

The chemical structure of PAMA was investigated by FTIR. The FTIR spectra of MA and PAMA are presented in Fig. S1. For MA, the multi-absorption peaks between 3100 and 3500 cm^{-1} belong to the $-NH_2$, and the numbers of peaks reduce to two in the FTIR spectrum of PAMA. The two relatively broaden peaks at 3361 and 3128 cm^{-1} are caused by the characteristic absorption of $-NH_3^+$ [36] and the overlay of a bit unreacted $-NH_2$. The bending vibration of $-NH_2$ in MA appears at 1654 cm^{-1}, while in PAMA it shifts to 1674 cm^{-1} due to the intermolecular interactions through the $-NH_2$ groups [37]. In comparison, a new absorption band, appearing at 1510 cm^{-1} for PAMA, can be ascribed to $-NH_3^+$ [38]. In addition, the breathing vibration of triazine ring in PAMA emerges at 776 cm^{-1}, which is much lower than that of MA (813 cm^{-1}), resulted by the characteristic iso form of the protonation of ring nitrogen [39]. This change further confirms the formation of ammonium salts. The peaks at 2922, 2855 and 1368 cm^{-1} are originated from the asymmetric, symmetric stretching and bending vibration of –CH–CH– on the ring structure of phytic acid, respectively. The characteristic absorption peaks at 1178 and 982 cm^{-1} are ascribed to the stretching vibration of P=O and the stretching vibration of P–O [40]. The peak at 1064 cm^{-1} is assigned to the stretching mode of $(PO3)^{2-}$ [41]. These characteristic absorption peaks reveal that a neutralization reaction does occur between phytic acid and melamine.

To further confirm the chemical formation of PAMA, the ^{1}H NMR of melamine and PAMA was carried out and shown in Fig. S2. As it can be seen, the peak at 2.50 ppm appears in both spectra of PAMA and MA, which comes from the solvent "DMSO-d_6". For MA, the resonance peak at 6.0 ppm originates from the protons of $-NH_2$. However, regarding to PAMA, the new peaks at 6.87 and 3.94 ppm appear, which can be ascribed to the $-NH_3^+$ protons and –CH–CH– protons in phytic acid, respectively, indicating the structure of melamine salt. It should be notable that the protons peaks of unreacted $-NH_2$ and P–OH disappear in the ^{1}H NMR spectrum of PAMA, which may be caused by the deuterium replacement by the strong polar solvent.

XPS is an effective method to reflect the atomic scale chemical interactions and provide reliable and quantifiable structural characteristic [42]. Aiming to comprehensively demonstrate the formation mechanism of PAMA, the XPS tests were performed for melamine and PAMA and the corresponding spectra are shown in Fig. 1. For PAMA, the new peaks located at 136.7, 193.9 and 535.1 eV are assigned to P_{2P}, P_{2S} and O_{1S} of PAMA, respectively. In addition, the fitted N_{1S} spectra are shown in Fig. 1 b, c and d. For MA (Fig. 1b), the N_{1s} peak at 398.3 eV is due to the –C=N-, and the N_{1s} peak at 399.1 eV corresponds to the $-NH_2$, which is consistent with Wang's report [43]. In the N_{1s} spectrum of PAMA (Fig. 1c), the N_{1s} peaks of MA still remain with a little shift of binding energy, but a new peak appears at 400.4 eV, which should be assigned to the N in $-NH_3^+$ [44]. At the same time, the integral area of –C=N- is nearly equal to the gross area of NH_2 and $-NH_3^+$; and the integral area of $-NH_3^+$ is almost twice as that of NH_2, which means that only two amino groups on triazine ring react with PA (shown in Scheme S1). Moreover, the fitted P_{2p} spectra are displayed in Fig. 1d. The spectrum of P_{2p} can be subdivided into 2 fitted peaks at 133.5 and 134.5 eV, assigned to HPO_4^{2-} and H_2PO^{4-}, respectively [45]. It is worth noting that the integral area of HPO_4^{2-} is five times that of H_2PO^{4-}, stating that the actual reaction molar ratio of MA: PA is 5: 1 (shown in Scheme S1). Further, the element contents of PAMA are shown in Table S1. The data show that the ratio of N/P in experimental value is 4.8: 1, which is approximate to the calculated value of 5: 1. All the results of ^{1}H NMR and XPS demonstrate that the hyperbranched PAMA molecules should have been synthesized successfully.

In general, the changes in the chemical structure will lead to some changes in crystal structure. Therefore, the crystal structure of PAMA was further investigated by means of X-ray diffraction. Fig. S3 shows the XRD patterns of MA and PAMA. For MA, the characteristic basal reflections appear at 2θ = 12.96, 14.70, 17.54, 21.50, 21.90, 26.04, 28.66 and 29.66°, indicating that MA is a typical monoclinic system [JCPDS No. 24-1654]. However, after reacted with phytic acid, the characteristic reflections of MA almost disappear and a series of new reflections at 2θ = 8.95, 9.76, 14.16, 15.16, 17.94, 18.52, 19.22, 20.84, 22.17, 24.32, 25.70, 27.19 and 27.99° appear in the XRD pattern of PAMA. The reason may be attributed to the high degree of hybridization between phytic acid and melamine, which leads to the destruction of the inherent crystal structure of MA and formed new state of aggregation. Based on the strong reflections of PAMA, an attempt of indexing the XRD pattern was undertaken by the Bragg equation ($2d\sin\theta = n\lambda$). The reflection peaks at 2θ = 8.95, 14.16, 17.94, 18.52, 19.22, 20.84, 22.17, 24.32, 25.70 and 27.19° can be assigned to ammonium hydrogen phosphate (JCPDS No. 16-0804). The reflection peak at 27.99°, corresponding to an inter-planar distance of 0.318 nm, indicating an obvious the π-π stacking of the aromatic triazine rings located in adjacent hyperbranched approximating planar molecules of PAMA, resulting in 2-D nano-layered structure [46]. What's more, an in-planar repeat period of 0.58 nm (100), corresponding to the distances of adjacent triazine rings around PA group in the PAMA molecules, is evident from the XRD reflection peak at 15.16°. Another repeat period of the same structural unit containing five triazine rings and one PA group also exists and results in the reflection peak at 9.76° (0.90 nm). All the XRD data show that the formation of the nano-layered structure with periodic triazine rings in the plane of hyperbranched PAMA molecules under the effect of π-π stacking [19] and hydrogen bonding (see Scheme S1 3-D structure of PAMA).

In order to confirm the presumed nano–layered stacking

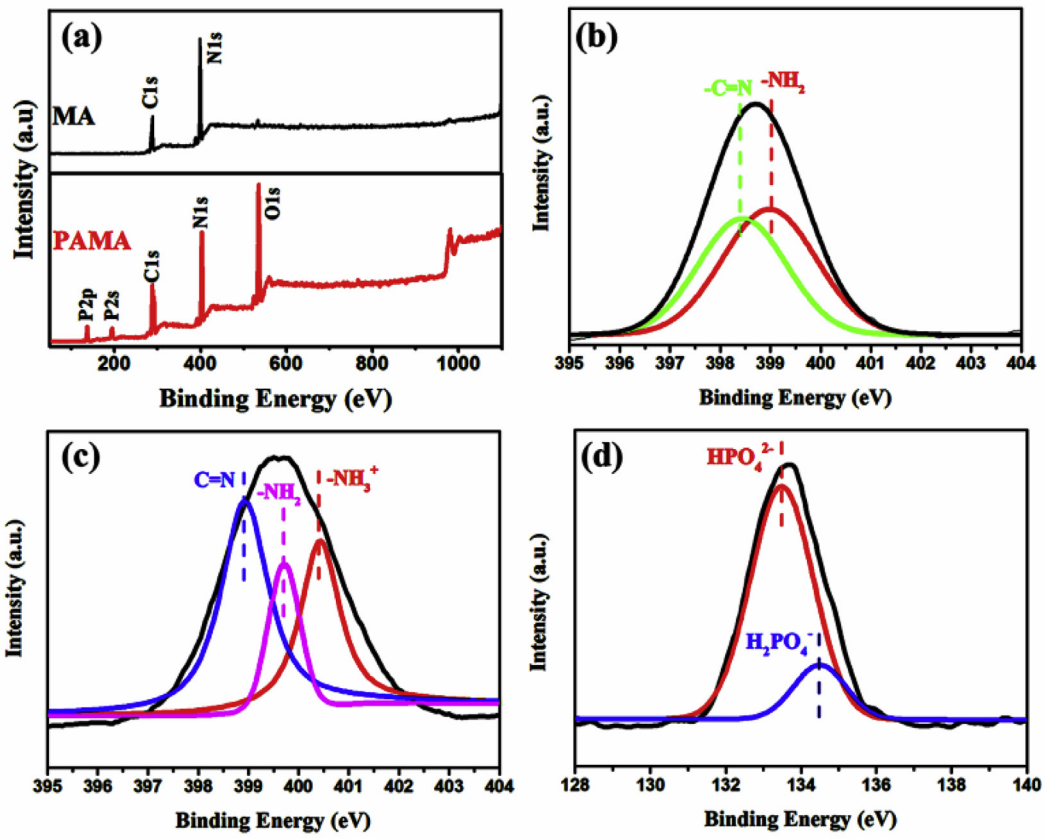

Fig. 1. Overall XPS spectra of MA and PAMA (a); N_{1s} spectra of (b) MA, (c) PAMA and (d) the various P_{2P} spectra of PAMA.

structure, SEM testing was used to investigate the morphology of MA and PAMA prepared under optimum reaction condition. The MA particles (Fig. S4) show a typical monoclinic crystal structure and its size is about 10 μm. However, it is surprising that the PAMA (Fig. 2a, a1) shows a petaloid nano-layered structure and the average diameter is less than 5 μm and the thickness is about 30 nm. The morphologies of PAMA under different reaction conditions were also investigated by SEM (see SI). The TEM images (Fig. 2b and b1) of PAMA reveal clearly the nano-layered structure, which means PAMA consisted of planes stacking along the c-axis. The planes are mainly constructed from the π-π stacking of triazine rings and hydrogen bonding resulted from unreacted $-NH_2$ and −OH, as shown in the inset of Fig. 2 b.

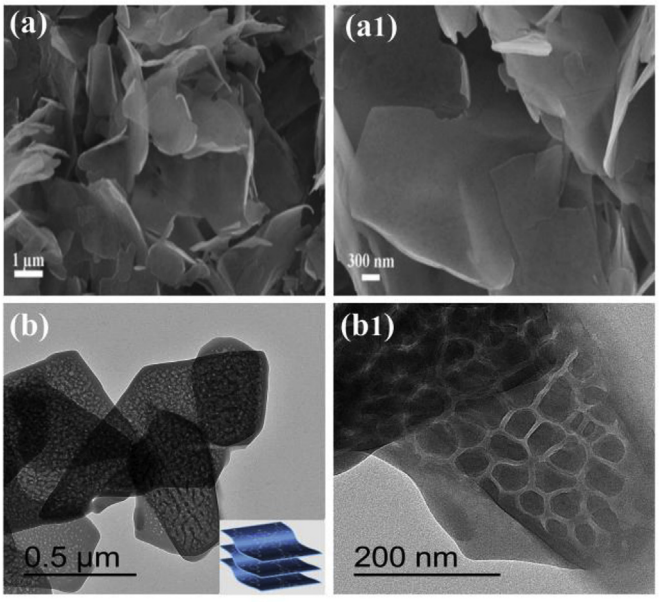

Fig. 2. (a, a1) SEM images and (b, b1) TEM images of PAMA.

To comprehensively understand the chemical formation of nano-lamellar PAMA, the EDX and EDX mapping tests of PAMA were carried out. The EDX results and EDX elements mapping images are shown in Fig. S5. Fig. S5 shows that the lamellar layer of PAMA is composed of C, N, O, and P elements. Moreover, the EDX elements mapping images reveal that the C, N, O, and P elements distribute evenly, further demonstrating that PAMA is formed by re-assemble in an orderly fashion, not a physical mixture of PA and MA.

Based on the above analysis, we can speculate about the growth mechanism of nano-layered PAMA. Firstly, the phytic acid reacts with the melamine to form the ammonium hydrogen phosphate by neutralization reaction, then producing hyperbranched macromolecules owing to the multi-functional groups of PA and MA; subsequently, the layer-by-layer self-assembling occurs under optimum condition, leading to produce the nano-layered PAMA under the effect of π-π stacking, hydrogen bonding. Consequently, the ideal schematic illustration for producing nano-layered PAMA is shown in Scheme S1.

In general, the dispersion performance of flame retardant additive is a crucial factor to affect the flame retardancy and mechanical properties. The SEM test was used to observe the

dispersion of PAMA and the corresponding result is shown in Fig. S6. EP-6 composite shows a typical brittle rupture and no obvious caves on the cross-section, indicating that PAMA lamellas possess good compatibility in the epoxy resin matrix, which is attributed to the organic group and the reactive groups existing in the PAMA molecules. This result was further demonstrated by the EDX Mapping image in Fig. S6 (a1), the even distribution of P signal manifests a homogeneous dispersion of PAMA lamellas in the epoxy matrix. However, for EP-7, some granular aggregates appear and the distribution of P element is not uniform (Fig. S6) which may be caused by the agglomeration of more PAMA. The glass-transition temperature (T_g) is an important parameter for characterizing the molecular chain structure. In principle, reactive additives with polymeric and rather rigid molecular structures will improve the T_g [47]. The T_g values of the EP and its composites were measured using DSC in a nitrogen atmosphere at 10 °C/min and the result is presented in Fig. S7. The T_g value for the EP is 122 °C. However, when adding the 6 wt% PAMA, the T_g value of EP-6 significantly increase to 135 °C, which can be explained by the incorporation of bulky and rigid structure of nano-layered PAMA. What's more, the $-NH_2$ group derived from PAMA can react with epoxy group, increasing the crosslinking density, consequently, limit the mobility of the molecular chain of EP [48]. It should be noticed that only one T_g appears after incorporated 6 wt% PAMA in EP, illuminating a uniform system of EP-6, which is consistent with the results of SEM.

Usually, the thermal degradation process of polymer will become more complex in air, and more weight loss occurs. The real combustion cycle of polymer material needs O_2, but the O_2 mainly exists in the region of the outer flame during burning; hence, it is close to the anaerobic environment rather than the aerobic environment at the interface between the flame and the surface of the underlying polymeric material during actual combustion. Accordingly, we merely discuss the thermal degradation process of PAMA under a nitrogen atmosphere rather than an air atmosphere.

The thermal degradation behaviours of PAMA, EP-0 and EP-6 were investigated by TG/DTG in N_2, and the TG and DTG curves are shown in Fig. 3. The corresponding data are summarized in Table S2, including the initial decomposition temperature ($T_{-5\%}$, 5% weight loss), the temperature at maximum weight loss rate (T_{max}) and the char residues at 600 and 700 °C. For PAMA, the thermal decomposition possesses two main degradation stages, and the $T_{-5\%}$ is 265.5 °C, at which point the decomposition of some thermally unstable structural groups in PAMA starts [49]. The first temperature at maximum weight loss rate (T_{max1}) is 282.9 °C, which can be assigned to the elimination of NH_3 and H_2O. Actually, During the temperatures range from 250 to 450 °C, the thermal decomposition of melamine and the dehydration reaction of phosphoric acid groups in phytic acid keep occurring slowly, generating the water vapor, NH_3, polyphosphoric acid, metaphosphoric acid, ammonium polyphosphate and melem polyphosphate by branching and crosslinking [49]. The second temperature at maximum weight loss rate (T_{max2}) appears at about 576.8 °C, corresponding to the release of phosphoric acid, polyphosphoric acid, metaphosphoric acid with the further decomposition of PAMA [50–53]. It should be noted that the residue of PAMA at 700 °C is 37.5% and PAMA exhibits a very low decomposition rate in the whole thermal degradation process, demonstrating that the PAMA possesses a high thermally stability. For EP (EP-0), it shows a single thermal decomposition stage starting at 362.4 °C, and almost immediately reaches its T_{max} at 397.4 °C with a maximum degradation rate of 1.62 wt %/min and a char residue of 17.94% at 700 °C. Compared with EP-0, EP-6 shows a lower $T_{-5\%}$, T_{max} and a higher char residue (22.98%) at 700 °C. The earlier thermal decomposition of EP-6 is mainly caused by the decomposition in advance of PAMA, which produces polyphosphoric acid and metaphosphoric acid, then accelerating the decomposition of EP matrix. During the high temperature stage, polyphosphoric acid and metaphosphoric acid can produce branched and cross-linking reaction and catalyze carbonization of EP molecules to form a stable protective char layer [54]. The maximum thermal degradation rate of EP-6 (1.19 wt%/°C) is much lower than that of EP-0, suggesting that introducing the PAMA into EP can effectively improve the thermal stability of EP. At the same time, the NH_3 and water derived from the decomposition of PAMA, serving as a blowing agent, can dilute the combustible gas and lead to the formation of effective intumescent char residue, which would protect the underlying matrix and thereby improve the fire resistance of EP composites [55]. Additionally, it is very noticeable that the T_{max2} at 576.8 °C of PAMA disappears in the DTG curve of EP-6, strongly corroborating the chemical crosslinking interaction between PAMA and EP molecules during curing process.

The limiting oxygen index (LOI) and UL-94 test results are presented in Table 1. EP-0 is highly combustible with a LOI value of 24% and is not classified in the UL-94 vertical test. However, the LOI values of EP/PAMA composites show a **gradual** improvement with increasing loadings of nano-lamellar PAMA. Particularly, by adding 6 wt% PAMA, the LOI value of EP-6 reaches 29.7% and the V-0 rating can be easily achieved. What's more, EP-7 shows a higher LOI value of 30.6% and reaches the V-0 rating in UL-94 test. The improved fire retardancy could be due to the physical barrier effect of nano-lamellar PAMA in condensed phase, the catalyzed carbonization effect of polyphosphoric acid produced by the thermal decomposition of PAMA, and the dilute and blowing effect of the non-combustible gases originated from melamine. Although EP-7 has the best LOI value, the improvement is not remarkable compared to

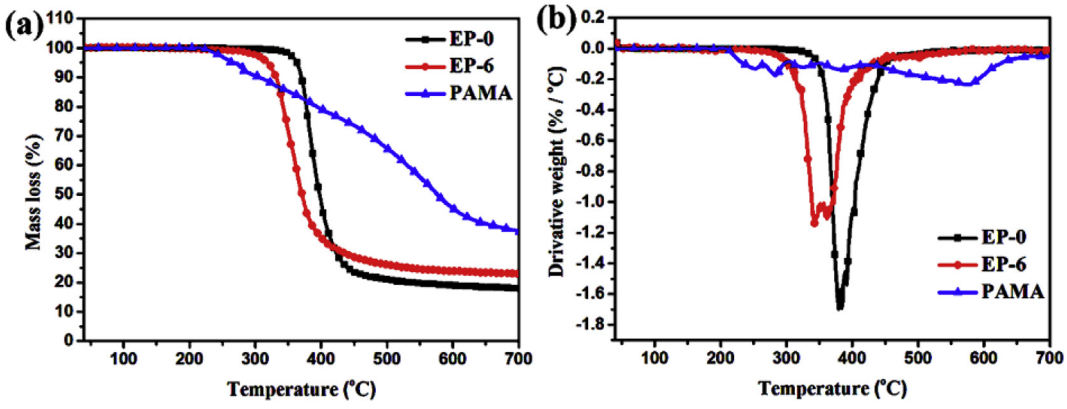

Fig. 3. (a) TG and (b) DTG curves of PAMA, EP-0, and EP-6 at a heating rate of 10 °C min^{-1} under N_2 atmosphere.

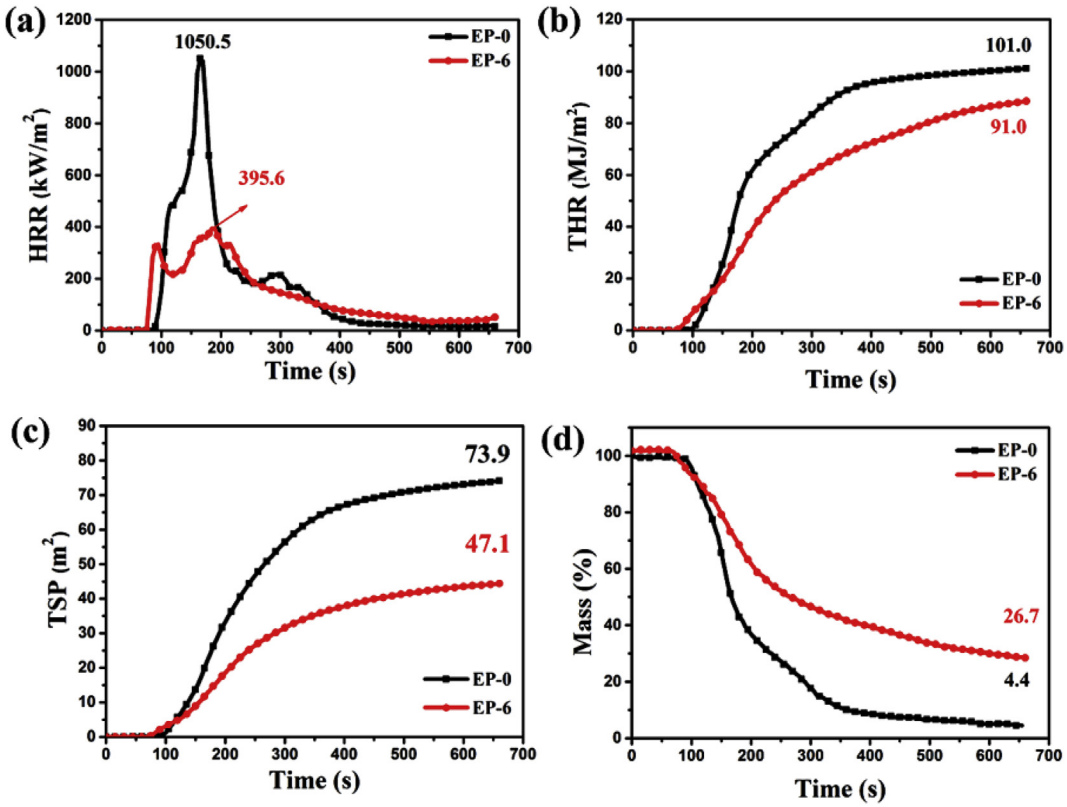

Fig. 4. (a) HRR, (b) THR, (c) TSP and (d) Mass loss curves of EP-0 and EP-6.

EP-6. Furthermore, the EP-6 has better tensile strength and impact strength than that of EP-7 (discussed following) and would be a more useful material. With a view to the balance between the fire retardancy and mechanical performance, EP-0 and EP-6 composites were selected to do the cone calorimeter test for further evaluating the fire behaviour of EP/PAMA composites.

The cone calorimeter (CC) is an effective method to evaluate the fire behaviour of polymeric material. The fire resistance performance of EP-0 and EP-6 were further investigated by cone calorimeter and the heat release rate (HRR), total heat release (THR), total smoke production (TSP) and mass loss rate curves are demonstrated in Fig. 4, and the corresponding data are shown in Table 2. Based on Fig. 4a and b, EP-0 burns rapidly after ignition and the peak heat release rate (PHRR) and THR are 1050.5 kW/m^2 and 101 MJ/m^2, respectively. Comparatively, the PHRR of EP-6 is remarkably reduced to 395.6 kW/m^2 (approximate 62.3% reduction) and the THR decreases to 91 MJ/m^2, suggesting that the addition of the nano-layered PAMA can significantly reduce the fire risk.

From the data in Table 2, it can be found that the time to ignition (TTI) of EP-6 occurs slightly earlier, which may be caused by the early decomposition of PAMA. The AvMLR of EP-6 shows a dramatic reduction from 17.21 to 6.02 g/s, suggesting that the early decomposition of PAMA makes for the formation of a protective stable char layer on the surface, which is well consistent with the TG/DTG results. The fire growth rate (FIGRA, FIGRA= PHRR/time to PHRR) is usually used to assess the fire hazards of the material. In general, a lower FIGRA implies a longer time to flashover, meaning that there is enough time to evacuate for people in fire danger [55]. The FIGRA value of EP-0 is 6.37 kW/m^2.s. However, the EP-6 exhibits a 62.16% reduction in FIGRA, suggesting that adding the PAMA actually largely decrease the fire hazards of EP material. The total smoke production (TSP) curves of EP-0 and EP-6 are shown in Fig. 4c. It is found that the TSP of EP-6 decreases from 73.94 to 47.1 m^2, stating that PAMA is also an effective smoke-suppression agent.

It should be noted that the char residue of EP after CC test is only 4.4% and but the char residue of EP-6 is 26.7%. This marked improvement in char residue further indicates that the addition of PAMA could effectively fix the carbon and promote partial epoxy molecules to be involved in the charring process, thereby improving the fire retardancy of the EP. This result can be verified by CO and CO_2 production of EP-0 and EP-6. Fig. S8 a and b, show a lower production of CO_2 and CO of EP-6 than that of EP-0, disclosing an obvious flame retardant mechanism of condensed phase action with more carbon fixed char residue [56]. However, the peaks of CO and CO_2 for EP-6 occurred earlier than EP-0. The reason may be attributed to the early decomposition of PAMA, and resulting in the formation of the stable protective char layer, which can prevent the EP matrix from further thermal degradation. Consequently, the smaller CO and CO_2 were formed during the combustion process of

Table 2
Detailed CC data of EP-0 and EP-6.

Samples	TTI (s)	PHRR (kW/m^2)	TTPHRR (s)	AvHRR (kW/m^2)	THR (MJ/m^2)	TSP (m^2)	Char (%)	AvMLR (g/s)	FIGRA (kW/m^2.s)
EP-0	72 ± 2	1050.5 ± 60	165 ± 3.5	172.7 ± 11.0	101.0 ± 1.8	73.9 ± 4.3	4.4 ± 1.0	17.2 ± 1.2	6.4 ± 0.3
EP-6	70 ± 2	395.6 ± 5.5	185 ± 10.6	116.7 ± 9.4	91.0 ± 1.2	47.1 ± 2.0	26.7 ± 1.4	6.0 ± 0.8	2.1 ± 0.2

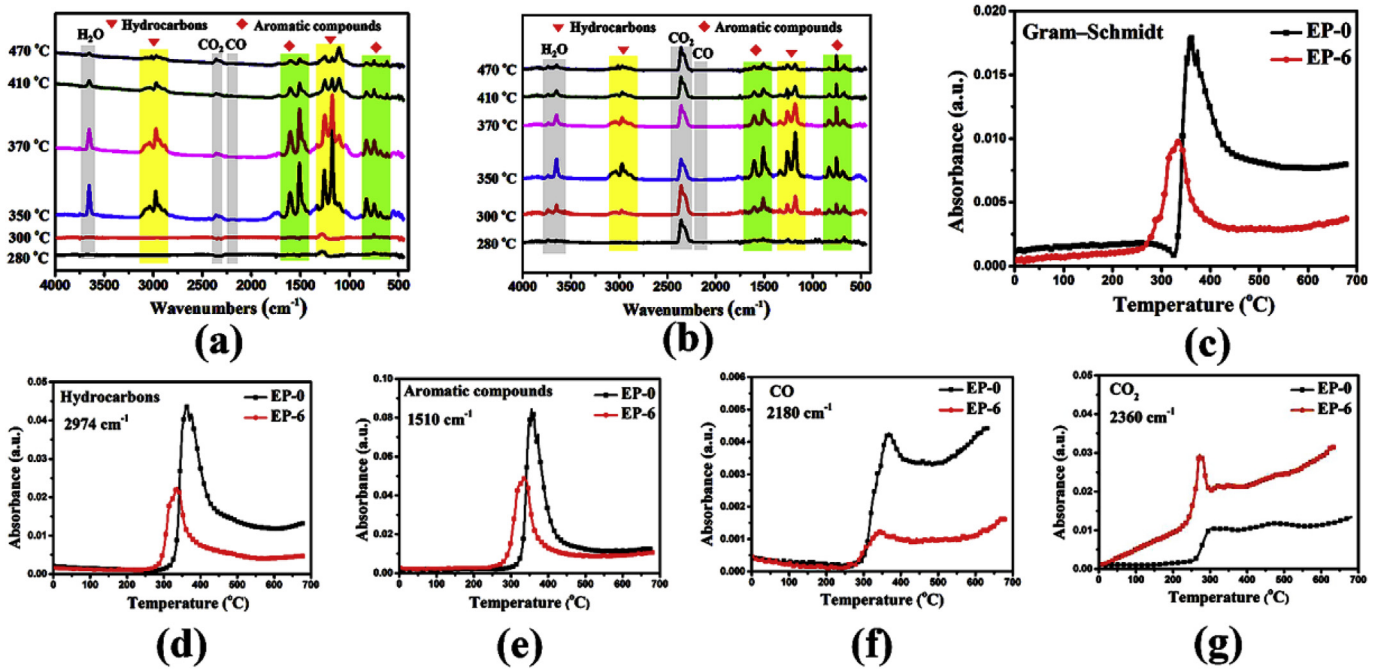

Fig. 5. (a, b) FTIR spectra of pyrolysis gaseous products for EP-0 and EP-6 at different stages of decomposition; Absorbance of pyrolysis products for EP-0 and EP-6 versus temperature: (c) Gram-schmidt (GS) curves, (d) hydrocarbons, (e) aromatic compounds (f) CO and (g) CO_2.

EP-6. Above all, PAMA is not only a good flame retardant but also in an effective smoke-suppression agent. The real-time TG-FTIR technique is the most popular method to determine gaseous products analysis during the thermal degradation process, which could make a great contribution to understanding the thermal degradation mechanism and the gas phase fire retarding mechanism.

The evolved gaseous volatiles of EP-0 and EP-6 are both recorded by TG-FTIR at a heating rate of 10 °C min^{-1} under nitrogen, and the corresponding FTIR spectra at different thermal degradation temperatures are shown in Fig. 5(a and b). It is found that there are almost similar gaseous products evolved from EP-0 and EP-6, such as H_2O (3600-4000 cm^{-1}), CO_2 (2360 cm^{-1}), CO (2180 cm^{-1}), hydrocarbons (2800-3000 cm^{-1}), and aromatic compounds (1605, 1510, 834, 748, and 689 cm^{-1}) [57,58]. Nevertheless, the maximum absorptions of all the pyrolysis gaseous products appear at 350 °C for EP-0, while the relevant maximum absorptions for the EP-6 shift to the earlier temperature owing to the earlier thermal degradation of nano-layered PAMA. The earlier thermal decomposition of PAMA might result in many nano-sized carbonization layers during combustion, which would act as a barrier for the transfer of heat and oxygen, consequently, protecting the underlying polymer matrix from further thermal degradation.

To understand thoroughly the influence of PAMA on the pyrolysis products of EP, the FTIR absorbance of pyrolysis products for EP-0 and EP-6 versus temperatures are shown in Fig. 5(c–g). Fig. 5 c presents the Gram-Schmidt (GS) curves as well as total volatile gas intensity versus the temperature curves of EP-0 and EP-6. It is clearly observed that EP-6 shows a lower gas pyrolytic products release, indicating the lower smoke toxicity. Furthermore, Fig. 5(d) and (e) and (f) display the absorbance intensity of hydrocarbons, aromatic compounds and CO of EP-0 and EP-6, which of EP-6 is much lower than that of EP-0. The result may be explained by two reasons: 1. The barrier effect of nano-sized carbonization layers formed by earlier thermal decomposition of PAMA; 2. Under a high temperature, the thermal decomposition product of PAMA, such as polyphosphoric acid, will promote the char-formation and consolidate more carbon in the condensed phase, thereby suppresses the further decomposition of EP. In general, hydrocarbons and aromatic compounds tend to aggregate into smoke particles [59], and CO is poisonous, which cause most fire accidents. The reduction of hydrocarbons, aromatic compounds and CO indicates

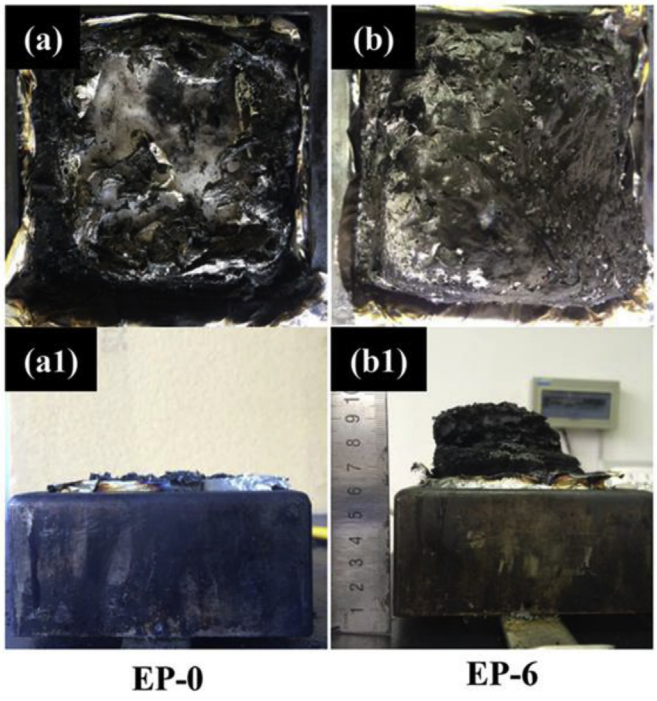

Fig. 6. The digital photographs of residual char after cone calorimeter test for (a, a1) EP-0 (b, b1) EP-6.

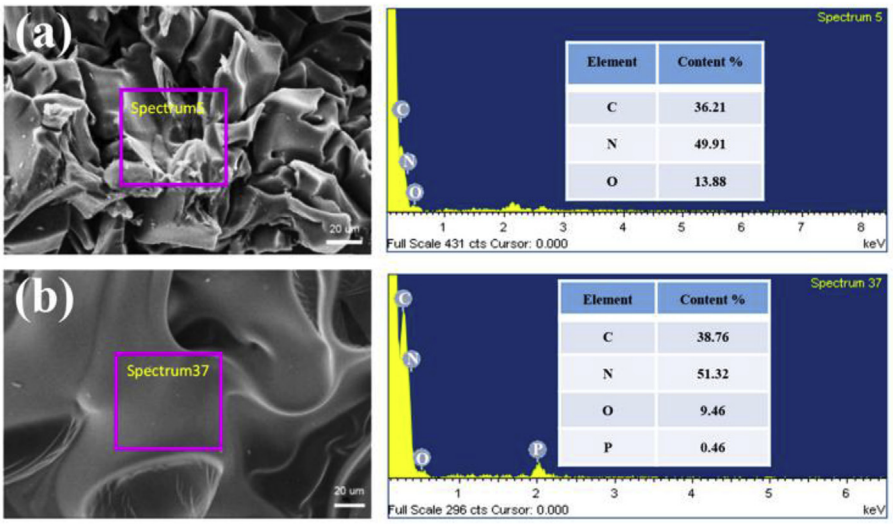

Fig. 7. SEM images of residues and corresponding EDX data for (a) EP-0, (b) EP-6.

fewer smoke particles and toxic gas formed during the thermal degradation, which will be conducive to fire rescue when a fire accident happens. One obvious increasing signal of CO_2 can be observed in Fig. 5 (b) and (g), which originates from the thermal degradation of PAMA starting from low temperature. The CO_2 is inert and dilute flammable gas, then preventing the further combustion of EP matrix, which is an important factor for the reduction of CO_2 of EP-6 in CC test. Therefore, the presence of PAMA could not only reduce and dilute flammable gas products, but also catalyze the more char formation of EP in the condensed phase.

Fig. 6 shows the digital photographs of residual char after cone calorimeter test for EP-0 and EP-6. Fig. 6 a and a1 show the EP-0 is almost burnt out. However, for EP-6, a denser and intumescent char layer can be observed from Fig. 6 b and b1, then reducing the heat and mass transfer between gas and condensed phases, which is agreement with the TG-FTIR data.

In order to further demonstrate the quality of the char residues, the char residues after cone calorimetry test were investigated by SEM as shown in Fig. 7. For EP-0, many cracks can be observed, meaning that the formed char cannot hinder heat and flammable gases. However, the char layer of EP-6 is continuous and compact (Fig. 7 b), which can provide a good barrier to the transfer of heat, oxide and flammable gases during combustion. This phenomenon may be the reason for the improvement of char residue, fire retardancy and smoke suppression of EP-6.

Additionally, the EDX was used to investigate the chemical elemental composition of the char residue of EP-0 and EP-6 after cone calorimetry test. As shown in Fig. 7, the change in the chemical components of the chars between EP-0 and EP-6 is also impressive. In general, the high ratio of C/O means that more carbons exist in the char residue, resulting in a better thermal oxidative resistance [60]. The C/O ratio of the residual char of EP-6 is 4.10, which is much higher than that of EP-0 (2.61), suggesting that the incorporation of PAMA does improve the thermal oxidative resistance of the char residue. There is no doubt that the char layer with high thermal oxidative resistance can hinder the heat transferring and mass loss, and thus significantly enhance the fire retardancy. Based on the above analysis, the possible flame retardant mechanism of EP-6 was shown in Scheme S2. From Scheme S2, in the early stage of combustion, the nano-layered PAMA forms firstly nano-sized carbonization layer, which acts as a barrier to delay the transfer of the heat and oxygen. Next, the various phosphorus-containing derivatives are produced from PAMA under high temperature, then accelerating the catalyzing carbonization of EP to form continuous, dense outer char layer and intumescent internal char layer, which could hinder the transfer of heat and oxygen and interrupt the flammable gas volatile feeding back to the combustion and thereby improve the fire resistance of EP-6. PAMA, a nano-lamellar filler with organic group is beneficial to improve the thermal stability and fire retardancy of EP like other nano-layered filler [32]. In summary, the PAMA, integrating the advantages of PA and MA, is really a promising candidate for a traditional intumescent flame retardant for EP.

The impact and tensile strength of EP and its composites were investigated (Fig. S9 and Table S3). And the stress-strain curve was shown in Fig. S10. Clearly, the impact strength of EP composites tends to decrease with the increased of the amount of the PAMA in the EP matrix, suggesting that the impact toughness of EP would be descent with the incorporation of PAMA. However, an increased tensile strength and Young Modulus of EP composites could be obtained when the addition of PAMA within 6 wt%. This result is attributed to factors: One is that the $-NH_2$ groups in PAMA molecules react with epoxy groups during the curing process, which will cause the higher density of cross-linking. In this case, the movement of molecule chains must be limited; the other is that the nano-lamellars of PAMA can restrict the segmental motion of the EP molecule chains. These factors are also reflected by the improved T_g value of EP-6 composite as discussed in DSC test (Fig. S7). In generally, nano-layered structure always shows the reinforcement effect in the polymer matrix [61–63]. However, for EP-7, its impact and tensile strength, as well as the Young Modulus are deteriorated, which can be explained by the agglomeration of PAMA as aforementioned in SEM (see Fig. S6).

4. Conclusions

In summary, in this work, a bio-based organic-inorganic hybrid with a unique nano-layered structure was first successfully synthesized via self-assembly and acting as an intumescent flame retardant used in epoxy resin. The T_g value of EP-6 was improved due to the rigid structure and the $-NH_2$ group derived from PAMA. The organic groups in PAMA endow its better dispersion performance in EP matrix. The results from TGA indicate that the PAMA exhibits an excellent thermal stability and the lamellar PAMA could

act as a barrier to delay the transfer of heat and promote carbonization of EP, thus improving the thermal stability of EP composites. The flame retardance and combustion behaviour of EP-6 and EP-0 were comprehensively investigated. With just 6 wt% loading of PAMA, the LOI value of EP-6 was increased to 29.7%, and the V-0 rating can be easily achieved. Moreover, the EP-6 composite exhibits a significant reduction in PHRR, THR, and TSP compared to that of EP-0 observed from CC test. The outstanding fire retardant and thermal stability properties of EP-6 over EP-0 are assigned to the unique nano-layered structure and the catalytic charring effects of PAMA, which is helpful to produce the compact and continuous residue char during combustion, consequently protect the underlying matrix from the fire. The tensile strength and Young Modulus of EP composites are enhanced by introducing less than or equal to 6 wt% PAMA when contrast to EP-0. The impact strength of EP composites decreases slightly compared to EP-0. These data show that PAMA is a green and multi-function nano-filler with efficient fire retardancy and mechanical reinforcement. This study can provide a new fire retarding idea to synthesize easily multi-function intumescent flame retardant with a nano-layered structure based on renewable resources.

Acknowledgements

This paper was financially supported by the National Natural Science Foundation of China (51673160; 51373140), The Project of State Key Laboratory of Environment-friendly Energy Materials, Southwest University of Science and Technology (17FKSY0116) and Longshan Academic Talent Research Support Plan of Southwest University of Science and Technology (17LZX404, 18LZX440).

Appendix A. Supplementary data

Supplementary data to this article can be found online at https://doi.org/10.1016/j.polymdegradstab.2018.11.024.

References

[1] W.C. Zhang, X.M. Li, R.J. Yang, Novel flame retardancy effects of DOPO-POSS on epoxy resins, Polym. Degrad. Stabil. 96 (2011) 2167–2173.
[2] L. Chen, S.G. Chai, K. Liu, N.Y. Ning, J. Gao, Q.F. Liu, F. Chen, Q. Fu, Enhanced epoxy/silica composites mechanical properties by introducing graphene oxide to the interface, ACS Appl. Mater. Interfaces 4 (2012) 4398–4404.
[3] J. Baller, N. Becker, M. Ziehmer, M. Thomassey, B. Zielinski, U. Müller, R. Sanctuary, Interactions between silica nanoparticles and an epoxy resin before and during network formation, Polymer 50 (2009) 3211–3219.
[4] C.M. Becker, A.D. Gabbardo, F. Wypych, S.C. Amico, Mechanical and flame-retardant properties of epoxy/Mg–Al LDH composites, Compos. Appl. Sci. Manuf. 42 (2011) 196–202.
[5] X.Y. Huang, C.Y. Zhi, P.K. Jiang, D. Golberg, Y. Bando, T. Tanaka, Polyhedral oligosilsesquioxane-modified boron nitride nanotube based epoxy nanocomposites: an ideal dielectric material with high thermal conductivity, Adv. Funct. Mater. 23 (2013) 1824–1831.
[6] C. Gérard, G. Fontaine, S. Bellayer, S. Bourbigot, Reaction to fire of an intumescent epoxy resin: protection mechanisms and synergy, Polym. Degrad. Stabil. 97 (2012) 1366–1386.
[7] S.Y. Lu, I. Hamerton, Recent developments in the chemistry of halogen-free flame retardant polymers, Prog. Polym. Sci. 27 (2002) 1661–1712.
[8] P.J. Wang, X.P. Hu, D.J. Liao, Y. Wen, T.R. Hull, F. Miao, Q.T. Zhang, Dual fire retardant action: the combined gas and condensed phase effects of azo-modified NiZnAl layered double hydroxide on intumescent polypropylene, Ind. Eng. Chem. Res. 56 (2017) 920–932.
[9] D.J. Liao, Q.K. Xu, R.W. McCabe, H.V. Babu, X.P. Hu, N. Pan, D.Y. Wang, T.R. Hull, Ferrocene-based nonphosphorus copolymer: synthesis, high-charring mechanism, and its application in fire retardant epoxy resin, Ind. Eng. Chem. Res. 56 (2017) 12630–12643.
[10] H.F. Yang, L. Ye, J. Gong, M.G. Li, Z. Jiang, X. Wen, H. Chen, N.N. Tian, T. Tang, Simultaneously improving the mechanical properties and flame retardancy of polypropylene using functionalized carbon nanotubes by covalently wrapping flame retardants followed by linking polypropylene, Mater. Chem. Front. 1 (2017) 716–726.
[11] I.Y. Jeon, S.H. Shin, H.J. Choi, S.Y. Yu, S.M. Jung, J.B. Baek, Heavily aluminated graphene nanoplatelets as an efficient flame-retardant, Carbon 116 (2017) 77–83.
[12] J.P. Han, G.Z. Liang, A.J. Gu, J.H. Ye, Z.Y. Zhang, L. Yuan, A novel inorganic–organic hybridized intumescent flame retardant and its super flame retarding cyanate ester resins, J. Mater. Chem. A. 1 (2013) 2169–2182.
[13] L.J. Qian, Y. Qiu, J.Y. Wang, W. Xi, High-performance flame retardancy by char-cage hindering and free radical quenching effects in epoxy thermosets, Polymer 68 (2015) 262–269.
[14] J.S. Wang, D.Y. Wang, Y. Liu, X.G. Ge, Y.Z. Wang, Polyamide-enhanced flame retardancy of ammonium polyphosphate on epoxy resin, J. Appl. Polym. Sci. 108 (2008) 2644–2653.
[15] X.P. Hu, Y.Y. Guo, L. Chen, X.X. Wang, L.J. Li, Y.Z. Wang, A novel polymeric intumescent flame retardant: synthesis, thermal degradation mechanism and application in ABS copolymer, Polym. Degrad. Stabil. 97 (2012) 1772–1778.
[16] L.N. Liu, M. Qian, P.A. Song, G.B. Huang, Y.M. Yu, S.Y. Fu, Fabrication of green lignin-based flame retardants for enhancing the thermal and fire retardancy properties of polypropylene/wood composites, ACS Sustain. Chem. Eng. 4 (2016) 2422–2431.
[17] S.K. Bondok, Y.A.M. Omaran, H.M.J. Abdel-Hamid, Enhanced productivity and quality of flame seedless grapevines treated with seaweed extract, J. Plant. Prod. 1 (2013) 1625.
[18] S. Pack, E. Bobo, N. Muir, K. Yang, S. Swaraj, H. Ade, C. Cao, C.S. Korach, T. Kashiwagi, M.H. Rafailovich, Engineering biodegradable polymer blends containing flame retardant-coated starch/nanoparticles, Polymer 53 (2012) 4787–4799.
[19] X.D. Jin, X.Y. Gu, C. Chen, W.F. Tang, H.F. Li, X.D. Liu, S. Bourbigot, Z.W. Zhang, J. Sun, S. Zhang, The fire performance of polylactic acid containing a novel intumescent flame retardant and intercalated layered double hydroxides, J. Mater. Sci. 52 (2017) 12235–12250.
[20] Z.H. Zheng, S.F. Liu, B.N. Wang, T. Yang, X.J. Cui, H.Y. Wang, Preparation of a novel phosphorus-and nitrogen-containing flame retardant and its synergistic effect in the intumescent flame-retarding polypropylene system, Polym. Compos. 36 (2015) 1606–1619.
[21] U. Braun, B. Schartel, M.A. Fichera, C. Jäger, Flame retardancy mechanisms of aluminium phosphinate in combination with melamine polyphosphate and zinc borate in glass-fibre reinforced polyamide 6, 6, Polymer Polym. Degrad. Stab. 92 (2007) 1528–1545.
[22] Z.Y. Wang, Y. Liu, Q. Wang, Flame retardant polyoxymethylene with aluminium hydroxide/melamine/novolac resin synergistic system, Polym. Degrad. Stabil. 95 (2010) 945–954.
[23] C.S. Wu, Y.L. Liu, Y.S. Chiu, Epoxy resins possessing flame retardant elements from silicon incorporated epoxy compounds cured with phosphorus or nitrogen containing curing agents, Polymer 43 (2002) 4277–4284.
[24] X.P. Hu, Y.L. Li, Y.Z. Wang, Synergistic effect of the charring agent on the thermal and flame retardant properties of polyethylene, Macromol. Mater. Eng. 289 (2004) 208–212.
[25] B. Bann, S.A. Miller, Melamine and derivatives of melamine, Chem. Rev. 58 (1958) 131–172.
[26] K. Apaydin, A. Laachachi, V. Ball, M. Jimenez, S. Bourbigot, V. Toniazzo, D. Ruch, Polyallylamine-montmorillonite as super flame retardant coating assemblies by layer-by layer deposition on polyamide, Polym. Degrad. Stabil. 98 (2013) 627–634.
[27] H.B. Yao, Z.H. Tan, H.Y. Fang, S.H. Yu, Artificial nacre-like bionanocomposite films from the self-assembly of chitosan-montmorillonite hybrid building blocks, Angew. Chem. Int. Ed. 49 (2010) 10127–10131.
[28] Z. Matusinovic, C.A. Wilkie, Fire retardancy and morphology of layered double hydroxide nanocomposites: a review, Angew. Chem. Int. Ed. 22 (2012) 18701–18704.
[29] Y.S. Gao, J.W. Wu, Q. Wang, C.A. Wilkie, D. O'Hare, Flame retardant polymer/layered double hydroxide nanocomposites, J. Mater. Chem. A. 2 (2014) 10996–11016.
[30] J.F. Ping, Y.X. Wang, Q.P. Lu, B. Chen, J.Z. Chen, Y. Huang, Q.L. Ma, C.L. Tan, J. Yang, X.H. Cao, Self-assembly of single-layer CoAl-layered double hydroxide nanosheets on 3D graphene network used as highly efficient electrocatalyst for oxygen evolution reaction, Adv. Mater. 28 (2016) 7640–7645.
[31] J.L. Gunjakar, T.W. Kim, H.N. Kim, I.Y. Kim, S.J. Hwang, Mesoporous layer-by-layer ordered nanohybrids of layered double hydroxide and layered metal oxide: highly active visible light photocatalysts with improved chemical stability, J. Am. Chem. Soc. 133 (2011) 14998–15007.
[32] C.L. Bao, L. Song, C.A. Wilkie, B.H. Yuan, Y.Q. Guo, Y. Hu, X.L. Gong, Graphite oxide, graphene, and metal-loaded graphene for fire safety applications of polystyrene, J. Mater. Chem. 22 (2012) 16399–16406.
[33] F. Kim, J.Y. Luo, R. Cruz-Silva, L.J. Cote, K. Sohn, J.X. Huang, Self-propagating domino-like reactions in oxidized graphite, Adv. Funct. Mater. 20 (2010) 2867–2873.
[34] W.X. Zhang, J.C. Cui, C.A. Tao, Y.G. Wu, Z.P. Li, L. Ma, Y.Q. Wen, G.T. Li, A strategy for producing pure single-layer graphene sheets based on a confined self-assembly approach, Angew. Chem. 121 (2009) 5978–5982.
[35] I.Y. Jeon, H.J. Choi, S.M. Jung, J.M. Seo, M.J. Kim, L. Dai, J.B. Baek, Large-scale production of edge-selectively functionalized graphene nanoplatelets via ball milling and their use as metal-free electrocatalysts for oxygen reduction reaction, J. Am. Chem. Soc. 135 (2013) 1386–1393.
[36] Y.H. Chen, Q. Wang, Reaction of melamine phosphate with pentaerythritol and its products for flame retardation of polypropylene, Polym. Adv. Technol. 18 (2007) 587–600.
[37] S.T. Huang, G.L. Wang, N.B. Li, H.Q. Luo, Mechanism of the pH-induced

aggregation reaction between melamine and phosphate, RSC Adv. 2 (2012) 10948.
[38] J.S. Maciel, D.A. Silva, H.C.B. Paula, R.C.M. de Paula, Chitosan/carboxymethyl cashew gum polyelectrolyte complex: synthesis and thermal stability, Eur. Polym. J. 41 (2005) 2726–2733.
[39] M. Scoponi, E. Polo, F. Pradella, V. Bertolasi, V. Carassiti, P. Goberti, Crystal structure and spectroscopic analysis of melamine hydrobromide. Evidence for iso-melamine cations and charge–transfer complexes in the solid state, J. Chem. Soc., Perkin Trans. 2 (7) (1992) 1127–1132.
[40] G.P. Jiang, J.L. Qiao, F. Hong, Application of phosphoric acid and phytic acid-doped bacterial cellulose as novel proton-conducting membranes to PEMFC, Int. J. Hydrogen Energy 37 (2012) 9182–9192.
[41] S.P. Valappil, D. Ready, E.A.A. Neel, D.M. Pickup, W. Chrzanowski, L.A. O'Dell, R.J. Newport, M.E. Smith, M. Wilson, J.C. Knowles, Antimicrobial gallium-doped phosphate-based glasses, Adv. Funct. Mater. 18 (2008) 732–741.
[42] I.D. Carja, D. Serbezeanu, T. Vlad-Bubulac, C. Hamciuc, A. Coroaba, G. Lisa, C.G. López, M.F. Soriano, V.F. Pérez, M.D. Romero Sánchez, A straightforward, eco-friendly and cost-effective approach towards flame retardant epoxy resins, J. Mater. Chem. A. 2 (2014) 16230–16241.
[43] G.J. Wang, J.Y. Yang, Thermal degradation study of fire resistive coating containing melamine polyphosphate and dipentaerythritol, Prog. Org. Coating 72 (2011) 605–611.
[44] D.M. Feng, Z.M. Zhou, M.P. Bo, An investigation of the thermal degradation of melamine phosphonite by XPS and thermal analysis techniques, Polym. Degrad. Stabil. 50 (1995) 65–70.
[45] X.F. Cui, Q.F. Li, Y. Li, F.H. Wang, G. Jin, M.H. Ding, Microstructure and corrosion resistance of phytic acid conversion coatings for magnesium alloy, Appl. Surf. Sci. 255 (2008) 2098–2103.
[46] X.C. Wang, K. Maeda, A. Thomas, K. Takanabe, G. Xin, J.M. Carlsson, K. Domen, M. Antonietti, A metal-free polymeric photocatalyst for hydrogen production from water under visible light, Nat. Mater. 8 (2009) 76–80.
[47] M. Ciesielski, A. Schäfer, M. Döring, Novel efficient DOPO-based flame-retardants for PWB relevant epoxy resins with high glass transition temperatures, Polym. Adv. Technol. 19 (2008) 507–515.
[48] G.R. Xu, M.J. Xu, B. Li, Synthesis and characterization of a novel epoxy resin based on cyclotriphosphazene and its thermal degradation and flammability performance, Polym. Degrad. Stabil. 109 (2014) 240–248.
[49] G. Camino, L. Costa, L. Trossarelli, Study of the mechanism of intumescence in fire retardant polymers: Part V-Mechanism of formation of gaseous products in the thermal degradation of ammonium polyphosphate, Polym. Degrad. Stabil. 12 (1985) 203–211.
[50] Z.B. Shao, C. Deng, Y. Tan, M.J. Chen, L. Chen, Y.Z. Wang, An efficient monocomponent polymeric intumescent flame retardant for polypropylene: preparation and application, ACS Appl. Mater. Interfaces 6 (2014) 7363–7370.
[51] Y. Tan, Z.B. Shao, L.X. Yu, J.W. Long, M. Qi, L. Chen, Y.Z. Wang, Piperazine-modified ammonium polyphosphate as monocomponent flame-retardant hardener for epoxy resin: flame retardance, curing behavior and mechanical property, Polym. Chem. 7 (2016) 3003–3012.
[52] Y. Tan, Z.B. Shao, L.X. Yu, Y.J. Xu, W.H. Rao, L. Chen, Y.Z. Wang, Polyethyleneimine modified ammonium polyphosphate toward polyamine-hardener for epoxy resin: thermal stability, flame retardance and smoke suppression, Polym. Degrad. Stabil. 131 (2016) 62–70.
[53] Y. Tan, Z.B. Shao, X.F. Chen, J.W. Long, L. Chen, Y.Z. Wang, Novel multifunctional organic–inorganic hybrid curing agent with high flame-retardant efficiency for epoxy resin, ACS Appl. Mater. Interfaces 7 (2015) 17919–17928.
[54] G. Laufer, C. Kirkland, A.B. Morgan, J.C. Grunlan, Intumescent multilayer nanocoating, made with renewable polyelectrolytes, for flame-retardant cotton, Biomacromolecules 13 (2012) 2843–2848.
[55] M. Gao, W.H. Wu, Y.Q. Yan, Thermal degradation and flame retardancy of epoxy resins containing intumescent flame retardant, J. Therm. Anal. Calorim. 95 (2009) 605–608.
[56] B. Schartel, T.R. Hull, Development of fire-retarded materials-Interpretation of cone calorimeter data, Fire Mater. 31 (2007) 327–354.
[57] N.H. Huang, J.Q. Wang, A TGA-FTIR study on the effect of $CaCO_3$ on the thermal degradation of EBA copolymer, J. Anal. Appl. Pyrolysis 84 (2009) 124–130.
[58] Y.Y. Dong, Z. Gui, Y. Hu, Y. Wu, S.H. Jiang, The influence of titanate nanotube on the improved thermal properties and the smoke suppression in poly (methyl methacrylate), J. Hazard Mater. 209 (2012) 34–39.
[59] D. Wang, L. Song, K.Q. Zhou, X.J. Yu, Y. Hu, J. Wang, Anomalous nano-barrier effects of ultrathin molybdenum disulfide nanosheets for improving the flame retardance of polymer nanocomposites, J. Mater. Chem. A. 3 (2015) 14307–14317.
[60] X. Wang, Y. Spörer, A. Leuteritz, I. Kuehnert, U. Wagenknecht, G. Heinrich, D.Y. Wang, Comparative study of the synergistic effect of binary and ternary LDH with intumescent flame retardant on the properties of polypropylene composites, RSC Adv. 5 (2015) 78979–78985.
[61] Z. Wang, T.J. Pinnavaia, Hybrid organic-inorganic nanocomposites: exfoliation of magadiite nanolayers in an elastomeric epoxy polymer, Chem. Mater. 10 (1998) 1820–1826.
[62] A. Dasari, Z.Z. Yu, Y.W. Mai, Nanoparticles, in: Polymer Nanocomposites, Springer, 2016, pp. 5–33.
[63] Y. Kim, J. Lee, M.S. Yeom, J.W. Shin, H. Kim, Y. Cui, J.W. Kysar, J. Hone, Y. Jung, S. Jeon, Strengthening effect of single-atomic-layer graphene in metal-graphene nanolayered composites, Nat. Commun. 4 (2013).